Structural Biological Materials: Critical Mechanics-Materials Connections

Marc André Meyers,[1,2]* Joanna McKittrick,[1] Po-Yu Chen[3]

Spider silk is extraordinarily strong, mollusk shells and bone are tough, and porcupine quills and feathers resist buckling. How are these notable properties achieved? The building blocks of the materials listed above are primarily minerals and biopolymers, mostly in combination; the first weak in tension and the second weak in compression. The intricate and ingenious hierarchical structures are responsible for the outstanding performance of each material. Toughness is conferred by the presence of controlled interfacial features (friction, hydrogen bonds, chain straightening and stretching); buckling resistance can be achieved by filling a slender column with a lightweight foam. Here, we present and interpret selected examples of these and other biological materials. Structural bio-inspired materials design makes use of the biological structures by inserting synthetic materials and processes that augment the structures' capability while retaining their essential features. In this Review, we explain this idea through some unusual concepts.

Materials science is a vibrant field of intellectual endeavor and research. This field applies physics and chemistry, melding them in the process, to the interrelationship between structure, properties, and performance of complex materials with technological applications. Thus, materials science extends these rigorous scientific disciplines into complex materials that have structures providing properties and synergies beyond those of pure and simple solids. Initially geared at synthetic materials, materials science has recently extended its reach into biology, especially into the extracellular matrix, whose mechanical properties are of utmost importance in living organisms. Some of the seminal work and important contributions in this field are either presented or reviewed in (*1*–*5*). There are a number of interrelated features that define biological materials and distinguish them from their synthetic counterparts [inspired by Arzt (*6*)]: (i) Self-assembly. In contrast to many synthetic processes to produce materials, the structures are assembled from the bottom up, rather than from the top down. (ii) Multi-functionality. Many components serve more than one purpose. For example, feathers provide flight capability, camouflage, and insulation, whereas bones provide structural framework, promote the growth of red blood cells, and provide protection to the internal organs. (iii) Hierarchy. Different, organized scale levels (nano- to ultrascale) confer distinct and translatable properties from one level to the next. We are starting to develop a systematic and quantitative understanding of this hierarchy by distinguishing the characteristic levels, developing constitutive descriptions of each level, and linking them through appropriate and physically based equations, enabling a full predictive understanding. (iv) Hydration. The properties are highly dependent on the level of water in the structure. There are some exceptions, such as enamel, but this rule applies to most biological materials and is of importance to mechanical properties such as strength (which is decreased by hydration) and toughness (which is increased). (v) Mild synthesis conditions. The majority of biological materials are fabricated at ambient temperature and pressure as well as in an aqueous environment, a notable difference from synthetic materials fabrication. (vi) Evolution and environmental constraints. The limited availability of useful elements dictates the morphology and resultant properties. The structures are not necessarily optimized for all properties but are the result of an evolutionary process leading to satisfactory and robust solutions. (vii) Self-healing capability. Whereas synthetic materials undergo damage and failure in an irreversible manner, biological materials often have the capability, due to the vascularity and cells embedded in the structure, to reverse the effects of damage by healing.

The seven characteristics listed above are present in a vast number of structures. Nevertheless, the structures of biological materials can be divided into two broad classes: (i) non-mineralized ("soft") structures, which are composed of fibrous constituents (collagen, keratin, elastin, chitin, lignin, and other biopolymers) that display widely varying mechanical properties and anisotropies depending on the function, and (ii) mineralized ("hard") structures, consisting of hierarchically assembled composites of minerals (mainly, but not solely, hydroxyapatite, calcium carbonate, and amorphous silica) and organic fibrous components (primarily collagen and chitin).

The mechanical behavior of biological constituents and composites is quite diverse. Biominerals exhibit linear elastic stress-strain plots, whereas the biopolymer constituents are nonlinear, demonstrating either a *J* shape or a curve with an inflection point. Foams are characterized by a compressive response containing a plastic or crushing plateau in which the porosity is eliminated. Many biological materials are composites with many components that are hierarchically structured and can have a broad variety of constitutive responses. Below, we present some of the structures and functionalities of biological materials with examples from current research. Here, we focus on three points: (i) How high tensile strength is achieved (biopolymers), (ii) how high toughness is attained (composite structures), and (iii) how bending resistance is achieved in lightweight structures (shells with an interior foam).

Structures in Tension: Importance of Biopolymers

The ability to sustain tensile forces requires a specific set of molecular and configurational conformations. The initial work performed on extension should be small, to reduce energy expenditure, whereas the material should stiffen close to the breaking point, to resist failure. Thus, biopolymers, such as collagen and viscid (catching spiral) spider silk, have a *J*-shaped stress-strain curve where molecular uncoiling and unkinking occur with considerable deformation under low stress.

This stiffening as the chains unfurl, straighten, stretch, and slide past each other can be represented analytically in one, two, and three dimensions. Examples are constitutive equations initially developed for polymers by Ogden (*7*) and Arruda and Boyce (*8*). An equation specifically proposed for tissues is given by Fung (*3*). A simpler formulation is given here; the slope of the stress-strain (σ-ε) curve increases monotonically with strain. Thus, one considers two regimes: (i) unfurling and straightening of polymer chains

$$\frac{d\sigma}{d\varepsilon} \propto \varepsilon^n (n > 1) \qquad (1)$$

and (ii) stretching of the polymer chain backbones

$$\frac{d\sigma}{d\varepsilon} \propto E \qquad (2)$$

where E is the elastic modulus of the chains. The combined equation, after integrating Eqs. 1 and 2, is

$$\sigma = k_1 \varepsilon^{n+1} + H(\varepsilon_c) E(\varepsilon - \varepsilon_c) \qquad (3)$$

Here k_1 is a parameter, and H is the Heaviside function, which activates the second term at $\varepsilon = \varepsilon_c$, where ε_c is a characteristic strain at which collagen fibers are fully extended. Subsequent strain gradually becomes dominated by chain stretching. The computational results by Gautieri *et al.* (*9*) on collagen fibrils corroborate Eq. 3 for $n = 1$. This corresponds to a quadratic relation between

[1]Department of Mechanical and Aerospace Engineering and Materials Science and Engineering Program, University of California, San Diego, La Jolla, CA 92093, USA. [2]Department of Nanoengineering, University of California, San Diego, La Jolla, CA 92093, USA. [3]Department of Materials Science and Engineering, National Tsing Hua University, Hsinchu 30013, Taiwan, Republic of China.

*To whom correspondence should be addressed. E-mail: mameyers@ucsd.edu

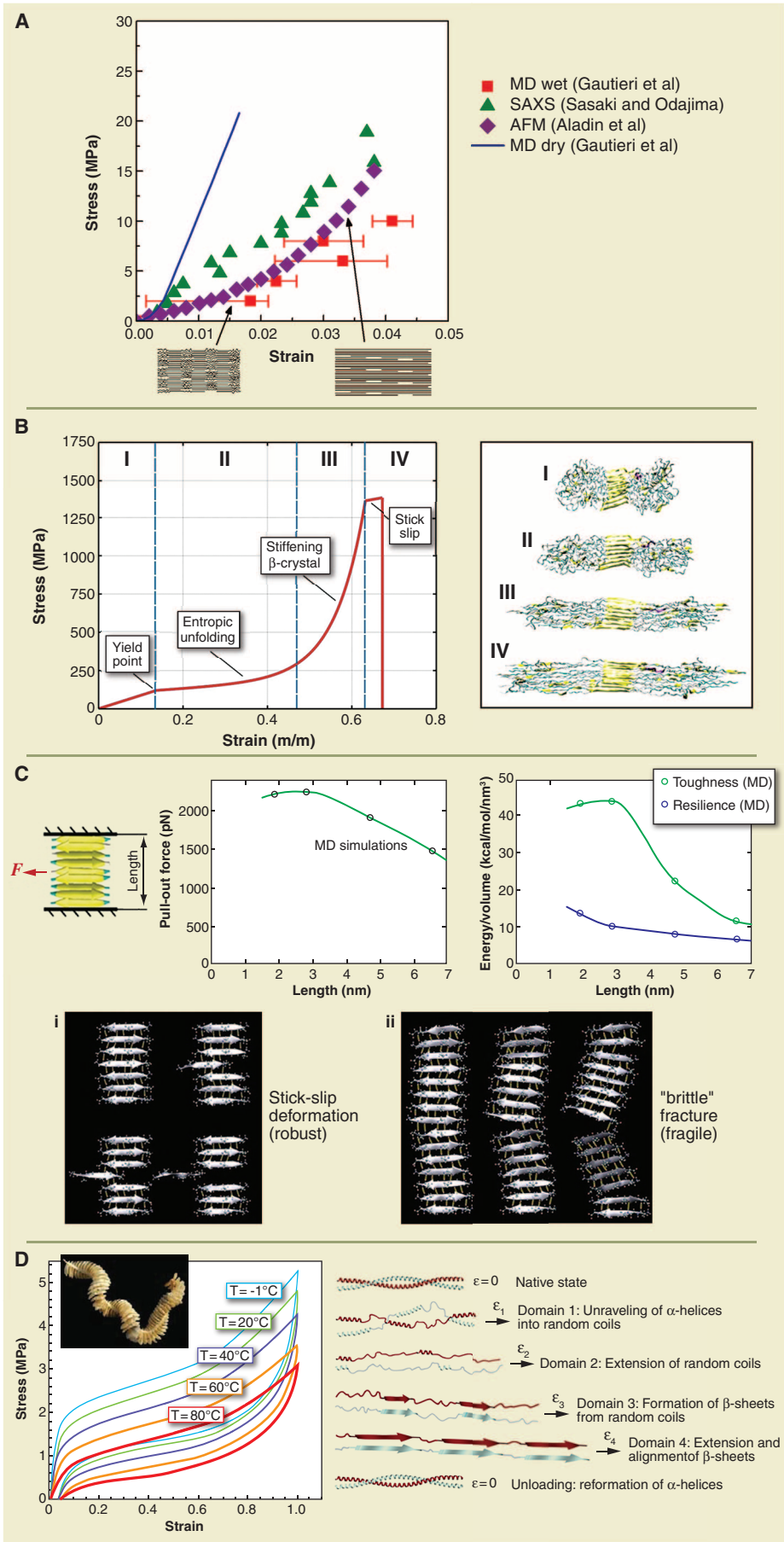

Fig. 1. Tensile stress-strain relationships in biopolymers. (**A**) *J*-shaped curve for hydrated and dry collagen fibrils obtained from molecular dynamics (MD) simulations and AFM and SAXS studies. At low stress levels, considerable stretching occurs due to the uncrimping and unfolding of molecules; at higher stress levels, the polymer backbone stretches. Adapted from (*9*, *12*). (**B**) Stretching of dragline spider silk and molecular schematic of the protein fibroin. At low stress levels, entropic effects dominate (straightening of amorphous strands); at higher levels, the crystalline parts sustain the load. (**C**) Molecular dynamics simulation of silk: (i) short stack and (ii) long stack of β-sheet crystals, showing that a higher pullout force is required in the short stack; for the long stack, bending stresses become important. Hydrogen bonds connect β-sheet crystals. Adapted from (*14*). (**D**) Egg whelk case (bioelastomer) showing three regions: straightening of the α helices, the α helix–to–β sheet transformation, and β-sheet extension. A molecular schematic is shown. Adapted from (*18*).

stress and strain ($\sigma \propto \varepsilon^2$), which has the characteristic *J* shape.

Collagen is the most important structural biological polymer, as it is the key component in many tissues (tendon, ligaments, skin, and bone), as well as in the extracellular matrix. The deformation process is intimately connected to the different hierarchical levels, starting with the polypeptides (0.5-nm diameter) to the tropocollagen molecules (1.5-nm diameter), then to the fibrils (~40- to 100-nm diameter), and finally to fibers (~1- to 10-μm diameter) and fascicles (>10-μm diameter). Molecular dynamics computations (*9*) of entire fibrils show the *J*-curve response; these computational predictions are well matched to atomic force microscopy (AFM) (*10*), small-angle x-ray scattering (SAXS) (*11*), and experiments by Fratzl *et al.* (*12*), as shown in Fig. 1A. The effect of hydration is also seen and is of great importance. The calculated density of collagen decreases from 1.34 to 1.19 g/cm^3 with hydration and is accompanied by a decrease in the Young's modulus from 3.26 to 0.6 GPa.

The response of silk and spider thread is fascinating. As one of the toughest known materials, silk also has high tensile strength and extensibility. It is composed of β sheet (10 to 15 volume %) nanocrystals [which consist of highly conserved poly-(Gly-Ala) and poly-Ala domains] embedded in a disordered matrix (*13*). Figure 1B shows the *J*-shape stress-strain curve and molecular configurations for the crystalline domains in silkworm (*Bombyx mori*) silk (*14*). Similar to collagen, the low-stress region corresponds to uncoiling and straightening of the protein strands. This region is followed by entropic unfolding of the amorphous strands and then stiffening due to load transfer to the crystalline β sheets. Despite the high strength, the major molecular interactions in the β sheets are weak hydrogen bonds. Molecular dynamics simulations,

shown in Fig. 1C, illustrate an energy dissipative stick-slip shearing of the hydrogen bonds during failure of the β sheets (*14*). For a stack with a height $L \leq 3$ nm (left-hand side of Fig. 1C), the shear stresses are more substantial than the flexure stresses, and the hydrogen bonds contribute to the high strength obtained (1.5 GPa). However, if the stack of β sheets is too high (right-hand side of Fig. 1C), it undergoes bending with tensile separation between adjacent sheets. The nanoscale dimension of the β sheets allows for a ductile instead of brittle failure, resulting in high toughness values of silk. Thus, size affects the mechanical response considerably, changing the deformation characteristics of the weak hydrogen bonds. This has also been demonstrated in bone (*15*–*17*), where sacrificial hydrogen bonds between mineralized collagen fibrils contribute to the excellent fracture resistance.

Other biological soft materials have more complex responses, marked by discontinuities in $d\sigma/d\varepsilon$. This is the case for wool, whelk eggs, silks, and spider webs. Several mechanisms are responsible for this change in slope; for instance, the transition from α- to β-keratin, entropic changes with strain (such as those prevalent in rubber, where chain stretching and alignment decrease entropy), and others. The example of egg whelk is shown in Fig. 1D (*18*). In this case, there is a specific stress at which α-keratin helices transform to β sheets, with an associated change in length. Upon unloading, the reverse occurs, and the total reversible strain is, therefore, extensive. This stress-induced phase transformation is similar to what occurs in shape-memory alloys. Thus, this material can experience substantial reversible deformation (up to 80%) in a reversible fashion, when the stress is raised from 2 to 5 MPa, ensuring the survival of whelk eggs, which are continually swept by waves.

These examples demonstrate the distinct properties of biopolymers that allow these materials to be strong and highly extensible with distinctive molecular deformation characteristics. However, many interesting biological materials are composites of flexible biopolymers and stiff minerals. The combination of these two constituents leads to the creation of a tough material.

Imparting Toughness: Importance of Interfaces

One hallmark property of most biological composites is that they are tough. Toughness is defined as the amount of energy a material absorbs before it fails, expressed as

$$U = \int_0^{\varepsilon_f} \sigma d\varepsilon \qquad (4)$$

where U is the energy per volume absorbed, σ is the stress, ε is the strain, and ε_f is the failure strain. Tough materials show considerable plastic deformation (or permanent damage) coupled with considerable strength. This maximizes the integral expression in Eq. 4. Biological composite materials (for example, crystalline and noncrystalline components) have a plethora of toughening mechanisms, many of which depend on the presence of interfaces. As a crack impinges on an interface or discontinuity in the material, the crack can be deflected around the interface (requiring more energy to propagate than a straight crack) or can drive through it. The strength of biopolymer fibers in tension impedes crack opening; bridges between microcracks are another mechanism. The toughening mechanisms have been divided into intrinsic (existing in the material ahead of crack) and extrinsic (generated during the progression of failure) categories (*19*). Thus, toughening is accomplished by a wide variety of stratagems. We illustrate this concept for four biological materials, shown in Fig. 2.

All inorganic materials contain flaws and cracks, which reduce the strength from the theoretical value (~E/10 to E/30). The maximum stress (σ_{max}) a material can sustain when a preexisting crack of length a is present is given by the Griffith equation

$$\sigma_{max} = \sqrt{\frac{2\gamma_s E}{\pi a}} = \frac{YK_{Ic}}{\sqrt{\pi a}} \qquad (5)$$

where E is the Young's modulus, γ_s is the surface (or damage) energy, and Y is a geometric parameter. $K_{Ic} = Y^{-1}\sqrt{2\gamma_s E}$ is the fracture toughness, a materials property that expresses the ability to resist crack propagation. Abalone (*Haliotis rufescens*) nacre has a fracture toughness that is vastly superior to that of its major constituent, monolithic calcium carbonate, due to an ordered assembly consisting of mineral tiles with an approximate thickness of 0.5 μm and a diameter of ~10 μm (Fig. 2A). Additionally, this material contains organic mesolayers (separated by ~300 μm) that are thought to be seasonal growth bands. The tiles are connected by mineral bridges with ~50-nm diameter and are separated by organic layers, consisting of a chitin network and acidic proteins, which, when combined, have a similar thickness to the mineral bridge diameters. The Griffith fracture criterion (Eq. 5) can be applied to predict the flaw size (a_{cr}) at which the theoretical strength σ_{th} is achieved. With typical values for the fracture toughness (K_{Ic}), σ_{th}, and E, the critical flaw size is in the range of tens of nanometers. This led Gao *et al*. (*20*) to propose that at sufficiently small dimensions (less than the critical flaw size), materials become insensitive to flaws, and the theoretical strength (~E/30) should be achieved at the nanoscale. However, the strength of the material will be determined by fracture mechanisms operating at all hierarchical levels.

The central micrograph in Fig. 2A shows how failure occurs by tile pullout. The interdigitated structure deflects cracks around the tiles instead of through them, thereby increasing the total length of the crack and the energy needed to fracture (increasing the toughness). Thus, we must determine how effectively the tiles resist pullout. Three contributions have been identified and are believed to operate synergistically (*21*). First, the mineral bridges are thought to approach the theoretical strength (10 GPa), thereby strongly attaching the tiles together (*22*). Second, the tile surfaces have asperities that are produced during growth (*23*) and could produce frictional resistance and strain hardening (*24*). Third, energy is required for viscoelastic deformation (stretching and shearing) of the organic layer (*25*).

One important aspect on the mechanical properties is the effect of alignment of the mineral crystals. The oriented tiles in nacre result in anisotropic properties with the strength and modulus higher in the longitudinal (parallel to the organic layers) than in the transverse direction. For a composite with a dispersed mineral m of volume fraction V_m embedded in a biopolymer (bp) matrix that has a much lower strength and Young's modulus than the mineral, the ratio of the longitudinal (L) and transverse (T) properties P (such as elastic modulus) can be expressed, in simplified form, as

$$\frac{P_L}{P_T} = \frac{P_m}{P_{bp}} V_m(1 - V_m) \qquad (6)$$

Thus, the longitudinal properties are much higher than the transverse properties. This anisotropic response is also observed in other oriented mineralized materials, such as bone and teeth.

Another tough biological material is the exoskeleton of an arthropod. In the case of marine animals [for instance, lobsters (*26*, *27*) and crabs (*28*)], the exoskeleton structure consists of layers of mineralized chitin in a Bouligand arrangement (successive layers at the same angle to each other, resulting in a helicoidal stacking sequence and in-plane isotropy). These layers can be envisaged as being stitched together with ductile tubules that also perform other functions, such as fluid transport and moisture regulation. The cross-ply Bouligand arrangement is effective in crack stopping; the crack cannot follow a straight path, thereby increasing the materials' toughness. Upon being stressed, the mineral components fracture, but the chitin fibers can absorb the strain. Thus, the fractured region does not undergo physical separation with dispersal of fragments, and self-healing can take place (*29*). Figure 2B shows the structure of the lobster (*Homarus americanus*) exoskeleton with the Bouligand arrangement of the fibers.

Bone is another example of a biological material that demonstrates high toughness. Skeletal mammalian bone is a composite of hydroxyapatite-type minerals, collagen and water. On a volumetric basis, bone consists of ~33 to 43 volume % minerals, 32 to 44 volume % organics, and 15 to 25 volume % water. The Young's modulus and strength increase, but the toughness decreases with increasing mineral volume fraction (*30*). Cortical (dense) mammalian bone has blood vessels extending along the long axis of the limbs. In animals larger than rats, the vessel is encased in a circumferentially laminated structure called the osteon. Primary osteons are surrounded by hypermineralized regions, whereas secondary

(remodeled) osteons are surrounded by a cement line (also of high mineral content) (*31*). In mammalian cortical bone, the following intrinsic toughening mechanisms have been identified: molecular uncoiling and intermolecular sliding of collagen, fibrillar sliding of collagen bonds, and microcracking of the mineral matrix (*19*). Extrinsic mechanisms are collagen fibril bridging, uncracked ligament bridging, and crack deflection and twisting (*19*). Rarely does a limb bone snap in two with smooth fracture surfaces; the crack is often deflected orthogonal to the crack front direction. In the case of (rehydrated) elk (*Cervus elaphus*) antler bone (shown in Fig. 2C) (*32*), which has the highest toughness of any bone type by far (*33*), the hypermineralized regions around the primary osteons lead to crack deflection, and the high amount of collagen (~60 volume %) adds mechanisms of crack retardation and creates crack bridges behind the crack front. The toughening effect in antlers has been estimated as: crack deflection, 60%; uncracked ligament bridges, 35%; and collagen as well as fibril bridging, 5% (*33*). A particularly important feature in bone is that the fracture toughness increases as the crack propagates, as shown in the plot. This plot demonstrates the crack extension resistance curve, or *R*-curve, behavior, which is the rate of the total energy dissipated as a function of the crack size. This occurs by the activation of the extrinsic toughening mechanisms. In this manner, it becomes gradually more difficult to advance the crack. In human bone, the cracks are deflected and/or twisted around the cement lines surrounding the secondary osteons and also demonstrate *R*-curve behavior (*34*).

The final example illustrating how the presence of interfaces is used to retard crack propagation is the glass sea sponge (*Euplectella aspergillum*). The entire structure of the Venus' flower basket is shown in Fig. 2D. Biological silica is amorphous and, within the spicules, consists of concentric layers, separated by an organic material, silicatein (*35*, *36*). The flexure strength of the spicule notably exceeds (by approximately fivefold) that of monolithic glass (*37*). The principal reason is the presence of interfaces, which can arrest and/or deflect the crack.

Biological materials use ingenious methods to retard the progression of cracks, thereby

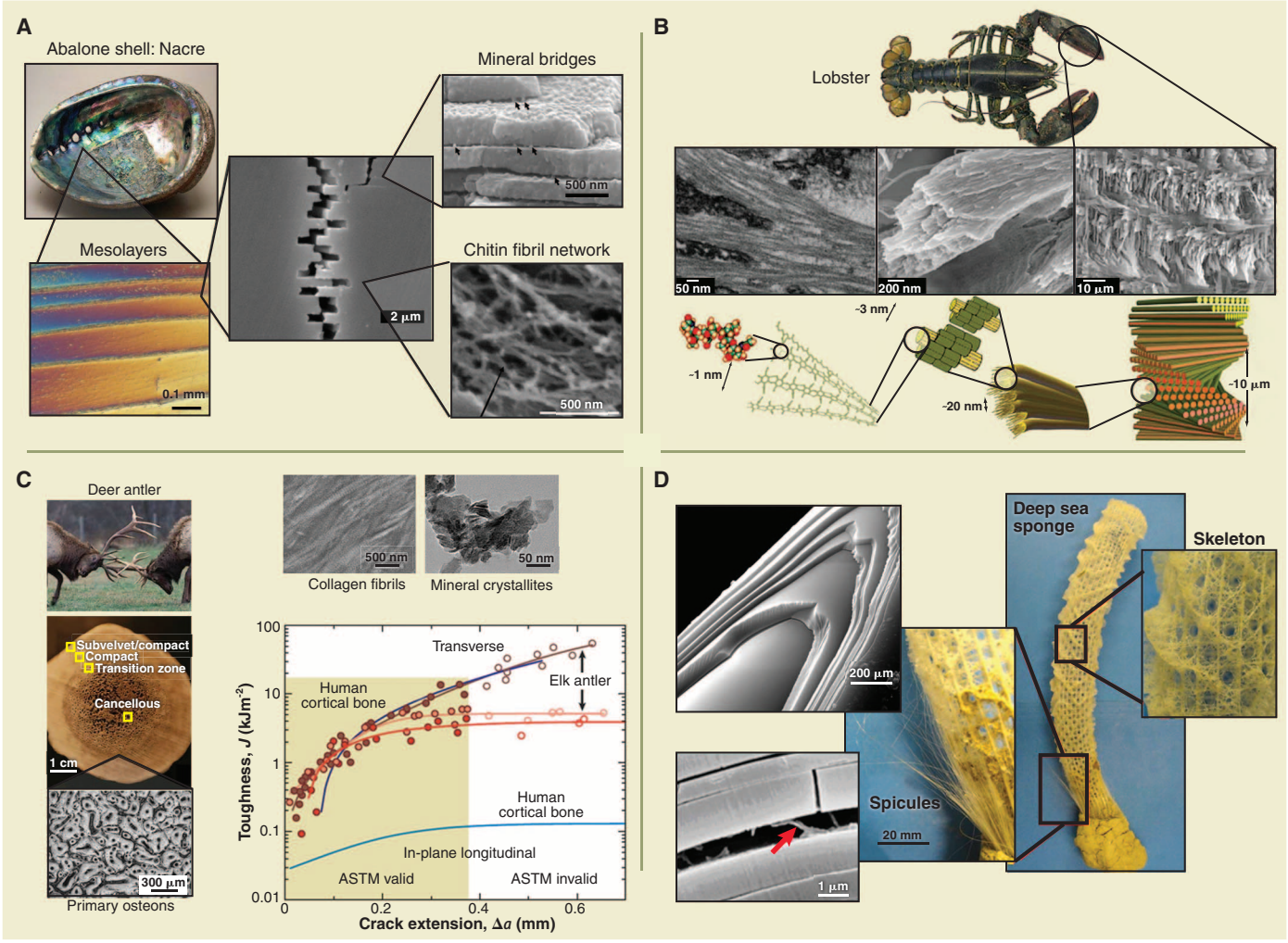

Fig. 2. Hierarchical structures of tough biological materials demonstrating the heterogeneous interfaces that provide crack deflection. (**A**) Abalone nacre showing growth layers (mesolayers), mineral bridges between mineral tiles and asperities on the surface, the fibrous chitin network that forms the backbone of the inorganic layer, and an example of crack tortuosity in which the crack must travel around the tiles instead of through them [adapted from (*4*, *21*)]. (**B**) Lobster exoskeleton showing the twisted plywood structure of the chitin (next to the shell) and the tubules that extend from the chitin layers to the animal [adapted from (*27*)]. (**C**) Antler bone image showing the hard outer sheath (cortical bone) surrounding the porous bone. The collagen fibrils are highly aligned in the growth direction, with nanocrystalline minerals dispersed in and around them. The osteonal structure in a cross section of cortical bone illustrates the boundaries where cracks perpendicular to the osteons can be directed [adapted from (*33*)]. ASTM, American Society for Testing and Materials. (**D**) Silica sponge and the intricate scaffold of spicules. Each spicule is a circumferentially layered rod: The interfaces between the layers assist in arresting crack propagation. Organic silicate in bridging adjacent silica layers is observed at higher magnification (red arrow) (*36*).

increasing toughness. These methods operate at levels ranging from the nanoscale to the structural scale and involve interfaces to deflect cracks, bridging by ductile phases (e.g., collagen or chitin), microcracks forming ahead of the crack, delocalization of damage, and others.

Lightweight Structures Resistant to Bending, Torsion, and Buckling—Shells and Foams

Resistance to flexural and torsional tractions with a prescribed deflection is a major attribute of many biological structures. The fundamental mechanics of elastic (recoverable) deflection, as it relates to the geometrical characteristics of beams and plates, is given by two equations: The first relates the bending moment, M, to the curvature of the beam, d^2y/dx^2 (y is the deflection)

$$\frac{d^2y}{dx^2} = \frac{M}{EI} \quad (7)$$

where I is the area moment of inertia, which depends on the geometry of the cross section ($I = \pi R^4/4$, for circular sections, where R is the radius). Importantly, the curvature of a solid beam, and therefore its deflection, is inversely proportional to the fourth power of the radius. The second equation, commonly referred to as Euler's buckling equation, calculates the compressive load at which global buckling of a column takes place (P_{cr})

$$P_{cr} = \frac{\pi^2 EI}{(kL)^2} \quad (8)$$

where k is a constant dependent on the column-end conditions (pinned, fixed, or free), and L is the length of the column. Resistance to buckling can also be accomplished by increasing I. Both Eqs. 7 and 8 predict the principal design

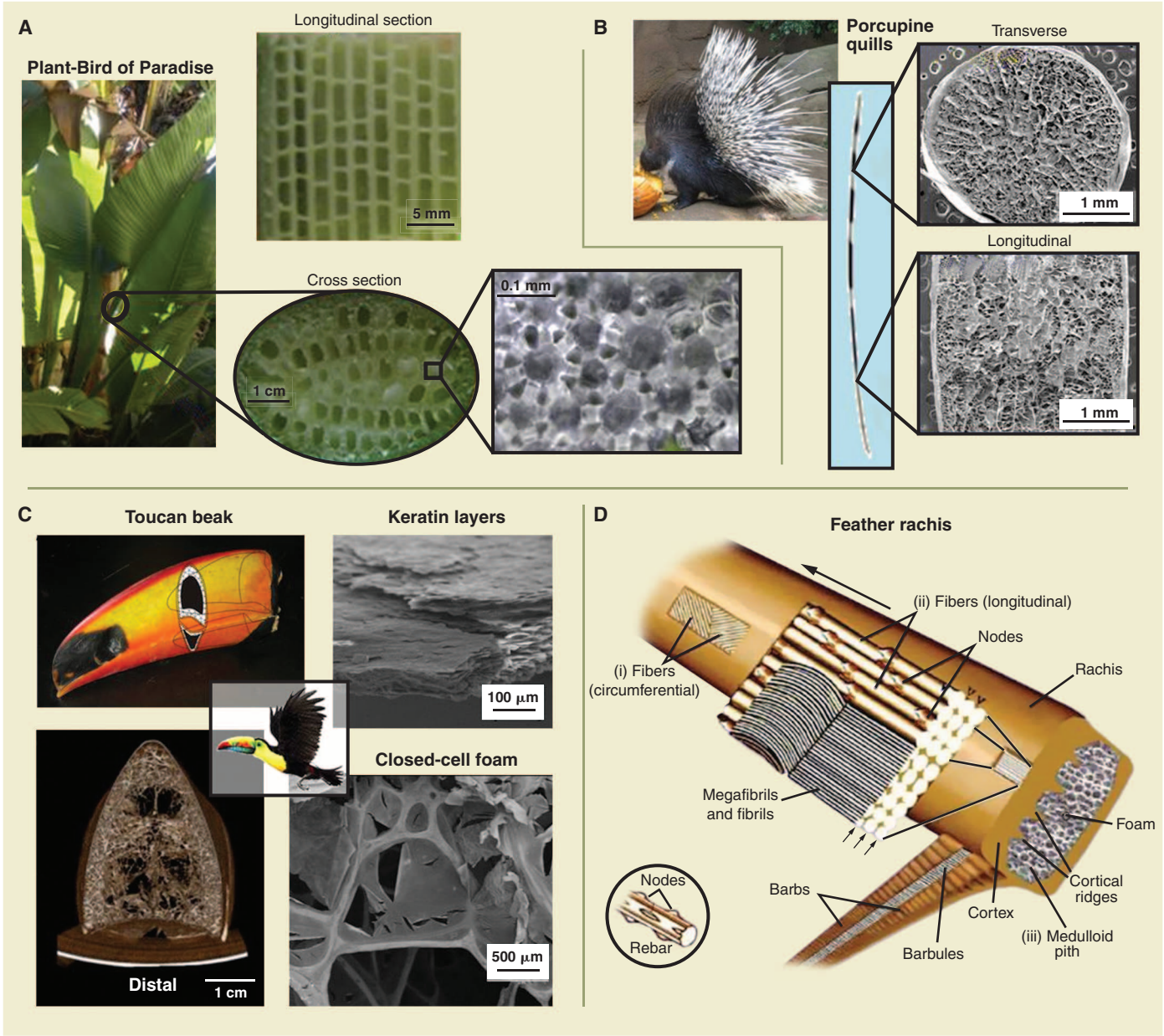

Fig. 3. Low-density and stiff biological materials. The theme is a dense outer layer and a low-density core, which provides a high bending strength–to–weight ratio. (**A**) Giant bird of paradise plant stem showing the cellular core with porous walls. (**B**) Porcupine quill exhibiting the dense outer cortex surrounding a uniform, closed-cell foam. Taken from (*42*). (**C**) Toucan beak showing the porous interior (bone) with a central void region [adapted from (*43*)]. (**D**) Schematic view of the three major structural components of the feather rachis: (i) superficial layers of fibers, wound circumferentially around the rachis; (ii) the majority of the fibers extending parallel to the rachidial axis and through the depth of the cortex; and (iii) foam comprising gas-filled polyhedral structures. Taken from (*45*).

guideline for a lightweight and/or stiff structure: For equal mass, I can be increased by placing the mass farthest from the neutral axis (that passes through the centroid of the cross section). This is readily accomplished by having a hollow tube with radius R and thickness t. For equal mass, $I_{tube}/I_{cylinder} = 1 + x^2$, where $x = 1 - t/R$. Thus, to increase bending resistance, t should be minimized and R maximized. However, the local buckling (crimping) tendency increases with an increase t and a decrease in R (*38*)

$$\sigma_{cr} = \frac{E}{\sqrt{3(1-\nu^2)}}\left(\frac{t}{R}\right) \quad (9)$$

where ν is Poisson's ratio. A compromise must be reached between bending and buckling resistance. The same reasoning can also be extended to torsion.

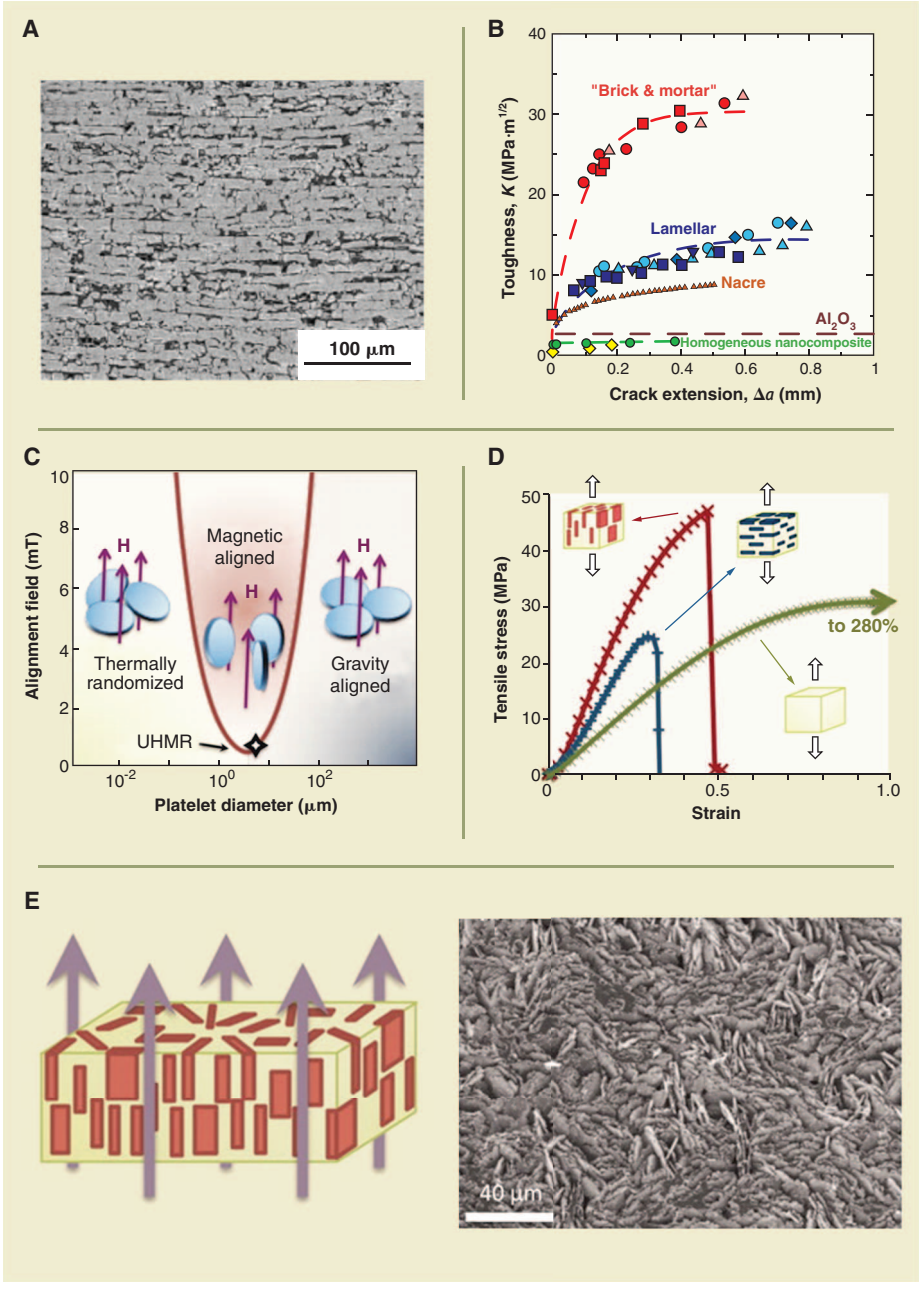

Fig. 4. Examples of bio-inspired designs. (**A**) Synthetic nacre consisting of alumina layers infiltrated with an engineering polymer and (**B**) crack propagation resistance [taken from (*56*)]. (**C**) Schematic diagram of platelet alignment in which magnetic fields are used to create a three-dimensional composite. UMHR, ultrahigh magnetic response; H, direction of magnetic field. (**D**) Stress-strain curves of a 20–volume % Al_2O_3 platelet-reinforced polyurethane with alignment parallel and perpendicular to the loading direction. The green curve shows the behavior of polyurethane. (**E**) Schematic representation (left) and SEM micrograph (right) of the composite. Taken from (*57*).

Nature has addressed this problem with ingenious solutions: creating a thin solid shell and filling the core with lightweight foam (*39*) or adding internal reinforcing struts or disks (*40*). These stratagems provide resistance to local buckling (crimping) with a minimum weight penalty. Primary examples of these design principles are antlers and some skeletal bones that have a cellular core (cancellous bone) and a solid exterior (cortical bone). Bamboo has a hollow tube with periodic disks at prescribed separations. The wing bones of soaring birds use this strategy with internal struts. Gibson and Ashby (*40*) and Gibson *et al.* (*41*) have covered this topic in detail.

To illustrate the ubiquity of this biological design principle, we present in Fig. 3 four additional examples: plants, porcupine quills, bird beaks, and feathers. Plant stalks are composed of cellulose and lignin arranged in cells aligned with the axis of growth. The giant bird of paradise (*Strelitzia*) (Fig. 3A) plant stem exhibits this structure. The longitudinal section shows rectangular cells, whereas the cell walls in the cross section are radially aligned. Thus, the cells have a cylindrical shape. The struts are not fully solid but instead have a pattern of holes, further decreasing the weight. The structure is designed to resist flexure stresses without buckling. Figure 3B shows the porcupine (*Hystrix cristata*) quill, a keratinous structure that has a high flexural strength-to-weight ratio (*42*). The external shell (cortex) surrounds a cellular core that provides stability to the walls under compression. This structure has a larger resistance to buckling than one in which the entire weight is concentrated on the external cortex (*39*).

Bird beaks are yet another example of this design principle. Beaks generally fall into two classes: short and thick or long and thin. The toucan (*Ramphastos toco*) is a notable exception; its beak is one third of its length and needs to be fairly thick for the foraging and fencing activities in the tree canopies. The beak is only $^1/_{30}$ of the bird's overall weight and has an extremely low density of 0.1 g/cm^3. The structure of the beak is fairly elaborate, with an external keratinous shell and an internal bony cellular structure (Fig. 3C) (*43*). The cells are composed of bony struts connected by membranes. An additional distinct feature of the toucan beak is a hollow core inside the foam, resulting in a further decrease in weight. The fundamental mechanics equation connecting the bending stresses in the radial distance, y, measured from the centroid is

$$\sigma_y = \frac{My}{I} \quad (10)$$

Because the stresses increase linearly with y, the central core does not experience substantial stresses and does not contribute to the flexure resistance; thus, nature removes the core.

Another example is the bird feather, which illustrates the extreme design considerations of the stiffness-to-weight ratio (*44*). Bird feathers are composed of a central shaft (rachis), out of which lateral branches (barbs) diverge. These

branches are connected by thin, folded membranes (barbules). We illustrate the structure of the rachis of a domestic chicken (*Gallus gallus*) in Fig. 3D (*45*). The entire feather is made of keratin; the external cortex is solid and is itself a composite, with longitudinal and circumferential layers of fibers. The core is filled with a closed-cell foam (level I). Close observation of the cell walls reveals that they are also made of a foam in a second level of porosity that further decreases density (level II). By applying an equation for a foam and assuming geometrical self-similarity, we have (*40*)

$$\frac{\rho_f}{\rho_s} = C\left(\frac{t}{l}\right)^4 \quad (11)$$

where ρ_f is the density of the foam, ρ_s is the density of the solid, C is a constant, t is the thickness of the cell struts, and l is the length of the struts (either level I or II). This fourth-order dependency demonstrates that the decrease in density accomplished by hierarchical foam of levels I and II is dramatic, as illustrated by the cortex foams of the feather rachis and bird of paradise flower.

The design principles delineated above—internal foams of various types and maximized moments of inertia—are used by biological systems in applications where the stiffness-to-weight ratio is of critical importance. Many engineering applications also use these concepts, but biological systems have distinct aspects (such as the hierarchical foam of the feather rachis) that are only at the conceptual stage at present but that may lead to substantial weight reduction.

Bio-Inspired Materials and Design

Due to the noteworthy physical and mechanical properties exhibited by biological materials, materials science has attracted considerable attention to the new research area of bio-inspiration. Some examples of bio-inspired materials design include Velcro (inspired by plant burrs), surfaces that are self-cleaning (super-hydrophobic surface of a lotus leaf) (*46*), antireflective surfaces of solar panels (insect compound eye) (*47*), fiber-reinforced composites (wood), and surfaces inspired by the structure of shark skin (*48*). Shark skin has small ridges separated by ~50 μm that are aligned in the direction of water flow. Instead of turbulent instabilities arising on the surface, a more laminar flow is achieved, which results in drag reduction (*48*). This concept has been applied to reduce drag in pipelines (*49*) and aircraft (*50*). Additionally, because of the surface roughness, bacterial colonies cannot develop; thus, a commercial product, Sharklet, is used in hospitals (*51*). Recent discoveries in the biomineralization area (*52*) and the gecko foot–inspired sticky tapes (*53*) are prime examples of new bio-inspired fabrication methods. Highly adhesive tapes have been demonstrated with carbon nanotubes and polymer nanopillars that reproduce the gecko foot setae structure (*54*, *55*). Thus, the field of bio-inspiration is generating innovations. However, it is challenging to fabricate bio-inspired materials that have structural function and robustness.

We have described two current efforts at creating structural bio-inspired materials. Mineralized biological materials have aligned mineral crystals that orient to maximize performance for required loading conditions; this concept is observed in bone, teeth, and mollusk shells. The abalone "brick-and-mortar" structure is an example of a tough material and is the subject of considerable research efforts. The most promising results have been obtained by freeze casting, a well-established ceramic processing method, followed by sintering and impregnation with a polymer or metal, as shown in Fig. 4A (*56*). The results are especially important, because the toughness obtained in a 80–volume % alumina, 20–volume % polymethyl methacrylate composite is very high: more than 30 MPa·m$^{1/2}$ (Fig. 4B). In comparison, pure alumina has a toughness of 2 to 3 MPa·m$^{1/2}$. With another method, Erb *et al*. (*57*) demonstrated alignment of alumina particles coated with superparamagnetic nanoparticles in a polyurethane matrix under a magnetic field (during solvent extraction from the polymer). Figure 4, C and D, shows a schematic representation of magnetic alignment of platelets and stress-strain curves of platelets oriented parallel and perpendicular to the loading direction, respectively. Figure 4E shows a scanning electron microscopy (SEM) micrograph and schematic rendition of the aligned particles—platelets orientated along the loading direction increase the yield strength and Young's modulus (Fig. 4, D and E). This concept was recently established by Porter *et al*. (*58*), who showed that the spiraling nature of the narwhal tusk could be reproduced by magnetic alignment of particles under a rotating magnetic field.

In conclusion, the application of the mechanics and materials science methodologies is promoting a new understanding of biological materials and guiding the design of biologically inspired materials and structures. This field is rapidly expanding, and we foresee a continued effort in bio-inspired materials and design, which will extend to sustainable development by employing more energy efficient and "greener" designs.

References and Notes

1. J. F. V. Vincent, *Structural Biomaterials* (Princeton University Press, Princeton, NJ, 1991).
2. A. H. Heuer *et al*., *Science* **255**, 1098 (1992).
3. Y. C. Fung, *Biomechanics: Mechanical Properties of Living Tissues* (Springer, New York, ed. 2, 1993).
4. M. A. Meyers, P.-Y. Chen, A. Y. M. Lin, Y. Seki, *Prog. Mater. Sci.* **53**, 1 (2008).
5. P.-Y. Chen, J. McKittrick, M. A. Meyers, *Prog. Mater. Sci.* **57**, 1492 (2012).
6. E. Arzt, *Mater. Sci. Eng. C* **26**, 1245 (2006).
7. R. W. Ogden, *Proc. R. Soc. London Ser. A Math. Phys. Sci.* **326**, 565 (1972).
8. E. M. Arruda, M. C. Boyce, *J. Mech. Phys. Solids* **41**, 389 (1993).
9. A. Gautieri, S. Vesentini, A. Redaelli, M. J. Buehler, *Nano Lett.* **11**, 757 (2011).
10. D. M. Aladin *et al*., *J. Orthop. Res.* **28**, 497 (2010).
11. N. Sasaki, S. Odajima, *J. Biomech.* **29**, 1131 (1996).
12. P. Fratzl *et al*., *J. Struct. Biol.* **122**, 119 (1998).
13. A. H. Simmons, C. A. Michal, L. W. Jelinski, *Science* **271**, 84 (1996).
14. S. Keten, Z. Xu, B. Ihle, M. J. Buehler, *Nat. Mater.* **9**, 359 (2010).
15. G. E. Fantner *et al*., *Nat. Mater.* **4**, 612 (2005).
16. J. B. Thompson *et al*., *Nature* **414**, 773 (2001).
17. J. D. Currey, *Nature* **414**, 699 (2001).
18. A. Miserez, S. S. Wasko, C. F. Carpenter, J. H. Waite, *Nat. Mater.* **8**, 910 (2009).
19. M. E. Launey, M. J. Buehler, R. O. Ritchie, *Annu. Rev. Mater. Res.* **40**, 25 (2010).
20. H. Gao, B. Ji, I. L. Jäger, E. Arzt, P. Fratzl, *Proc. Natl. Acad. Sci. U.S.A.* **100**, 5597 (2003).
21. A. Y. M. Lin, M. A. Meyers, *J. Mech. Behav. Biomed. Mater.* **2**, 607 (2009).
22. F. Song, Y. L. Bai, *Acta Mech. Sin.* **17**, 251 (2001).
23. T. E. Schäffer *et al*., *Chem. Mater.* **9**, 1731 (1997).
24. A. G. Evans *et al*., *J. Mater. Res.* **16**, 2475 (2001).
25. A. P. Jackson, J. F. V. Vincent, R. M. Turner, *Proc. R. Soc. London Ser. B Biol. Sci.* **234**, 415 (1988).
26. D. Raabe, C. Sachs, P. Romano, *Acta Mater.* **53**, 4281 (2005).
27. S. Nikolov *et al*., *Adv. Mater.* **22**, 519 (2010).
28. P.-Y. Chen, A. Y. M. Lin, J. McKittrick, M. A. Meyers, *Acta Biomater.* **4**, 587 (2008).
29. C. A. Melnick, Z. Chen, J. J. Mecholsky Jr., *J. Mater. Res.* **11**, 2903 (1996).
30. J. D. Currey, *Philos. Trans. R. Soc. London Ser. B Biol. Sci.* **304**, 509 (1984).
31. J. D. Currey, *Bone: Structure and Mechanics* (Princeton University Press, Princeton, NJ, 2002).
32. P.-Y. Chen, A. G. Stokes, J. McKittrick, *Acta Biomater.* **5**, 693 (2009).
33. M. E. Launey, P.-Y. Chen, J. McKittrick, R. O. Ritchie, *Acta Biomater.* **6**, 1505 (2010).
34. R. K. Nalla, J. J. Kruzic, J. H. Kinney, R. O. Ritchie, *Biomaterials* **26**, 217 (2005).
35. J. N. Cha *et al*., *Proc. Natl. Acad. Sci. U.S.A.* **96**, 361 (1999).
36. J. Aizenberg *et al*., *Science* **309**, 275 (2005).
37. L. Qiao, Q.-L. Feng, X.-H. Wang, Y.-M. Yang, *J. Inorg. Mater.* **23**, 337 (2008).
38. S. Timoshenko, *Theory of Elastic Stability* (McGraw-Hill, New York, 1936).
39. G. N. Karam, L. J. Gibson, *Int. J. Solids Struct.* **32**, 1259 (1995).
40. L. J. Gibson, M. F. Ashby, *Cellular Solids: Structure and Properties* (Cambridge Univ. Press, Cambridge, ed. 2, 1997).
41. L. J. Gibson, M. F. Ashby, B. Harley, *Cellular Materials in Nature and Medicine* (Cambridge Univ. Press, Cambridge, 2010).
42. W. Yang, C. Chao, J. McKittrick, *Acta Biomater.* **9**, 5297 (2013).
43. Y. Seki, M. S. Schneider, M. A. Meyers, *Acta Mater.* **53**, 5281 (2005).
44. P. P. Purslow, J. F. V. Vincent, *J. Exp. Biol.* **72**, 251 (1978).
45. T. Lingham-Soliar, R. H. C. Bonser, J. Wesley-Smith, *Proc. R. Soc. London Ser. B Biol. Sci.* **277**, 1161 (2010).
46. T. Sun, L. Feng, X. Gao, L. Jiang, *Acc. Chem. Res.* **38**, 644 (2005).
47. F. Chiadini, V. Fiumara, A. Scaglione, A. Lakhtakia, *Bioinspir. Biomim.* **5**, 026002 (2010).
48. J. Oeffner, G. V. Lauder, *J. Exp. Biol.* **215**, 785 (2012).
49. S.-J. Lee, H.-C. Lim, M. Han, S. S. Lee, *Fluid Dyn. Res.* **37**, 246 (2005).
50. P. R. Viswanath, *Prog. Aerosp. Sci.* **38**, 571 (2002).
51. www.sharklet.com
52. J. Aizenberg, *MRS Bull.* **35**, 323 (2010).
53. E. P. Chan, C. Greiner, E. Arzt, A. J. Crosby, *MRS Bull.* **32**, 496 (2007).
54. S. Sethi, L. Ge, L. Ci, P. M. Ajayan, A. Dhinojwala, *Nano Lett.* **8**, 822 (2008).
55. K. Jin *et al*., *Langmuir* **28**, 5737 (2012).
56. E. Munch *et al*., *Science* **322**, 1516 (2008).
57. R. M. Erb, R. Libanori, N. Rothfuchs, A. R. Studart, *Science* **335**, 199 (2012).
58. M. M. Porter *et al*., *Mater. Sci. Eng. A* **556**, 741 (2012).

Acknowledgments: We thank W. Yang and C.-H. Lu for help with the figures. This work is funded by the NSF, Ceramics Program grant 1006931 (M.A.M. and J.M.), and the National Science Council, Taiwan, grants NSC-100-2218-E-007-016-MY3 and NSC-101-2628-E-007-017-MY3 (P.-Y.C.).

10.1126/science.1220854

Science
AAAS

Structural Biological Materials: Critical Mechanics-Materials Connections

Marc André Meyers, Joanna McKittrick and Po-Yu Chen (February 14, 2013)

Science **339** (6121), 773-779. [doi: 10.1126/science.1220854]

Editor's Summary

The Building Blocks of Life

Biological organisms are often limited in the resources that they can use to make structural materials. Primary building blocks may be weak or brittle materials, such as minerals and biopolymers, and processing conditions by default have to be mild. Despite this, a wide range of strong and tough structures exist, including shells, bones, quills, and fibers. **Meyers *et al.*** (p. 773) review a wide range of materials and architectures used in nature to make strong and tough materials and show how many of the design principles have also been used or are being considered for manmade materials and structures.

Science (print ISSN 0036-8075; online ISSN 1095-9203) is published weekly, except the last week in December, by the American Association for the Advancement of Science, 1200 New York Avenue NW, Washington, DC 20005.